文章编号：1001-9014(2024)01-0106-10

DOI:10.11972/j.issn.1001-9014.2024.01.015

Infrared small target detection based on associated directional gradient and mean contrast

LI Ning[1], GUO Yi-Fang[1*], JIAO Ji-Chao[1], PANG Min[2], XU Wei[2]

(1. School of Electronic Engineering, Beijing University of Posts and Telecommunications, Beijing 100876, China;
2. Third Research Department, China Institute of Radio Propagation, Qingdao 266108, China)

Abstract: The detection of infrared small targets has been a challenging task in the field of computer vision due to the low percentage of small targets in the whole image and the presence of a large amount of clutter around the targets. We propose an algorithm based on associated directional gradient and mean contrast. The algorithm consists of two modules: the associated directional gradient module uses a Gaussian distribution model of infrared small targets, and adds the gradient in a single direction with the gradient in an adjacent direction to form a new feature called associated directional gradient, which enhances the real target, suppresses background clutter, and eliminates the effect of highlighting edges on the target detection. The mean contrast module incorporates directional information to calculate multi-directional contrast of the target. The minimum value of multi-directional contrast is chosen to suppress structural noise, and the idea of mean filtering is introduced into the calculation of contrast to suppress isolated noise in the background and further reduce the false alarm rate of detection. Experimental results on actual infrared images show that the algorithm can achieve better results in enhancing the signal-to-noise ratio of the target and suppressing the background noise.

Key words: infrared image, target detection, associated directional gradient, mean contrast

基于联合方向梯度和均值对比度的红外弱小目标检测方法

李 宁[1], 郭义放[1*], 焦继超[1], 逄 敏[2], 徐 威[2]

(1. 北京邮电大学 电子工程学院,北京 100876;
2. 中国电波传播研究所 第三研究部,山东 青岛 266108)

摘要:针对小目标在整幅图像中占比很低,且目标周围存在大量杂波,提出了一种基于联合方向梯度(Associated Directional Gradient,ADG)和均值对比度(Mean Contrast,MC)的红外弱小目标检测算法。该算法由两个模块组成:ADG利用红外弱小目标的高斯分布模型,将单一方向的梯度与一个相邻方向上的梯度相加组成新的联合梯度特征,增强真实目标、抑制背景杂波的同时能够消除高亮边缘对目标检测效果的影响;MC融入方向信息来计算目标的多方向对比度,选用多方向对比度的最小值抑制结构噪声,并将均值滤波的思想引入对比度的计算,抑制背景中的孤立噪声,进一步降低检测的虚警率。在实际红外图像上的实验结果表明,该算法在增强目标信噪比和抑制背景噪声方面,能够取得较好效果。

关 键 词:红外图像;目标检测;联合方向梯度;均值对比度

中图分类号:TP722.5　　**文献标识码**:A

Introduction

Infrared target detection has a wide range of applications in optical remote sensing, air defense early warning, and night surveillance. Especially in military application scenarios such as enemy aircraft tracking and minefield detection, where have various factors such as long imaging distance, low target pixel share, inherent sensor noise, and a complex natural environment background, make the detection of weak infrared targets very

Received date: 2023-07-12, **revised date**: 2023-11-03　　**收稿日期**:2023-07-12,**修回日期**:2023-11-03

Biography: LI Ning (1967-), female, Beijing, associate professor, PhD. Research area involves image information processing and satellite mobile communications. E-mail: Lnmmdsy@bupt.edu.cn

* **Corresponding author**: E-mail: yifang_guo@126.com

difficult[1-2].

In the past decades, a variety of methods have been proposed in the field of infrared small target detection[3-7]. Traditional infrared small target detection algorithms rely on background subtraction. Firstly, the background of the infrared target is predicted, and then the difference between the original infrared image and the background is calculated[8-10]. Deshpande et al[8] proposed maximum median filtering and maximum mean filtering to estimate the background. Although median filtering and mean filtering can suppress some of the burst noise, the detection effect is not satisfactory when the signal-to-noise ratio of the image is low. Zeng et al[9] first introduced top-hat morphological filtering into the field of infrared target detection for estimating the background to obtain a residual map, but it could not suppress background clutter and was very sensitive to noise. Bai et al[10] defined a novel top-hat transform and applied it to infrared small target detection, but the applicable scenario of the algorithm was very limited and could not be adapted to infrared targets of different sizes. Although the method based on background subtraction is simple to implement and efficient to detect, it lacks the use of features of the target which leads to the detection effect being hardly satisfactory.

Compared to visible images, infrared images lack features such as color and texture details, but the contrast is very obvious. Therefore, researchers began to work on using contrast features for infrared small target detection tasks[11-14]. Chen et al[15] first proposed the local contrast method (LCM) based on the human visual system. Han et al[16] improved the detection efficiency by modifying the definition of local contrast and defining pixel sub-blocks instead of pixel-by-pixel detection. Pan et al[17], inspired by LCM, designed a two-layer contrast model to expand the detection area of the nested structure to obtain more complete contrast information. The contrast-based approach is capable of enhancing the target, but the algorithm is very sensitive to pepper noise in the background because the maximum value of contrast is taken into account in the calculation.

Gradient features are also one of the research hotspots in the field of infrared small target detection[18-20]. Zhang et al[21] divided the detection structure into four quadrants of a two-dimensional coordinate system to locate the position of a small infrared target by calculating the pointing of the gradient of the pixel points. However, there is a lot of structural noise in the infrared image with similar structures to small targets, which has the same gradient pointing as the target in some directions, resulting in a high false alarm rate of the algorithm in complex backgrounds. The averaged absolute gradient[22] uses the property of local averaging to suppress background clutter and achieves a robust detection effect, but it lacks the use of directional information, and the algorithm cannot correctly detect the location of small targets when one side of the small target is near the highlighted edge. Saeid Aghaziyarati et al[23] weighted the directional derivative with the average absolute gray difference to address the effect of highlighting edges on the detection effect, but the detection performance of the algorithm decreases significantly when the pixel value of the target is low, or when there are multiple targets with large target brightness disparity in one image.

Based on the above problems, an algorithm based on associated directional gradient and mean contrast (*ADGMC*) is proposed in this paper:

(1) Four detection structures with different directions are designed to obtain the gray gradient between the target area and the surrounding background area, and the concept of "associated directional gradient" is proposed to suppress background noise and eliminate the effect of highlighting background edges on gradient changes.

(2) Based on the characteristic of "similar contrast in all directions" for small targets, the idea of mean filtering is used to construct a mean contrast detection structure to eliminate isolated noise and enhance the target at the same time.

(3) For the case that there exist multiple targets with large grayscale differences in one image, after calculating the associated directional gradient, the associated directional gradient feature map is nonlinearly mapped to ensure that the algorithm can detect all the small targets in the image completely.

1 Proposed Method

The method proposed in this paper consists of two main modules: the associated directional gradient module and the mean contrast module. First, in the associated directional gradient module, the gradient is redefined as the sum of the gradients in a single direction and adjacent directions, called the joint gradient. Based on the gradient distribution characteristics of the small target, four different detection structures are designed to obtain the associated directional gradient characteristics of the small target in different directions (up, down, left, and right). Second, considering the case that there are multiple small targets with large luminance differences in one image, a nonlinear mapping function is used to reduce the disparity of feature values between different targets. Then, in the mean contrast module, a contrast detection structure is designed based on the directionality of the small target grayscale distribution, and the minimum value of contrast in the four directions of small target is taken as the final contrast value. The idea of mean-filter is introduced into the calculation of contrast, which makes full use of the directionality of small target grayscale distribution and eliminates the influence of isolated noise on the detection results. Finally, a simple threshold segmentation method is used to segment the target. The flowchart of the *ADGMC* algorithm is shown in Fig. 1.

1.1 Calculation of Associated Directional Gradient

The traditional definition of gradient only focuses on the grayscale change in a single direction of the target, as shown in Fig. 2, when the target is close to the high-brightness edge, although the small target has high gradi-

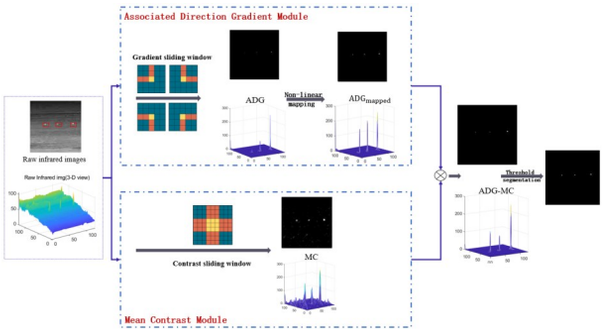

Fig. 1 flowchart of *ADGMC*
图1 ADGMC流程图

ents in the upper, left, and right directions, the lower side of the target is very close to the background high-brightness edge, and the gradient in that direction may plummet to zero.

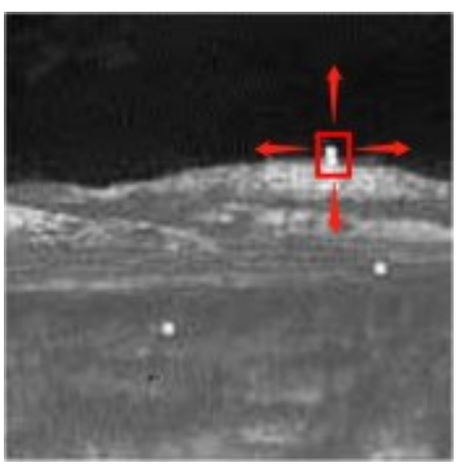

Fig. 2 target near the highlighted edge
图2 目标靠近高亮边缘

To solve the problem that the gradient is easily affected by the highlighted edges, this paper proposes the concept of associated directional gradient, redefining the gradient calculation from a single direction as the sum of the gradients of that direction and another adjacent direction. Four gradient detection structures are designed as shown in Fig. 3; T is the region where the target center is located, B1, and B2 are the background regions for calculating the associated gradients.

For the detection structures shown in Fig. 3, the associated directional gradient is defined as

$$Gradient = \sum_{(x,y)\in B1}\left(\left(x_T,y_T\right)-\left(x,y\right)\right)+\sum_{(x,y)\in B2}\left(\left(x_T,y_T\right)-\left(x,y\right)\right), \quad (1)$$

The sky background shown in Fig. 4(a) is one of the main application scenarios for IR small target detection. Assuming that the small target is surrounded by complex clouds and the brightness of the clouds exceeds that of the small target, the pixel distribution of the target and the background is shown in Fig. 4(b). The blue area is the area where the small target is located, the red

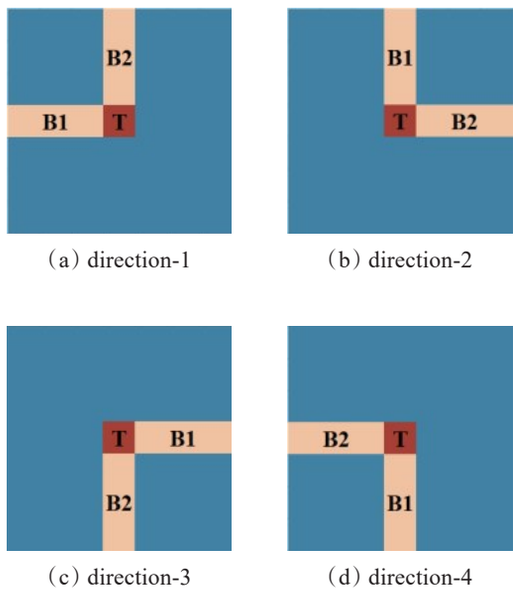

(a) direction-1 (b) direction-2

(c) direction-3 (d) direction-4

Fig. 3 Gradient detection structure of each associated direction (a) is the upper associate left, (b) is the upper associate right, (c) is the right associate lower, (d) is the lower associate left
图3 每个联合方向上的梯度检测结构 (a) 左上联合方向,(b)上右联合方向,(c)右下联合方向,(d)下左联合方向

pixel point denotes the brightest point of the small target, and the rest is the background area. Taking Fig. 3(a) as an example, it is assumed that the brightest point of the small target is exactly in the T area of the detection structure. Since the small target is surrounded by brighter clouds, if the size of the detection structure shown in Fig. 3(a) is 3*3, the return value of the upper-left associated gradient at this point is 25; if the detection structure size is 5*5, the return value will reduce to -5. But for the associated gradient at the bottom right of the target, because the background at the bottom right region is lower than the center of the small target, the larger the detection structure, the larger the gradient value returned.

(a) (b)

Fig. 4 Infrared small target near the highlighted edge (a) Local enlargement, (b) Pixel schematic
图4 红外小目标靠近高亮边缘 (a)局部放大图,(b)像素示意图

Considering various complex backgrounds, the multi-scale sizes of 3*3, 5*5 and 7*7 are set for the detection structures shown in Fig. 3, and the maximum val-

ue of the multi-scale is taken as the associated directional gradient value in that direction. Therefore, the multi-scale associated directional gradient is defined as

$$Gradient_{n*n} = max\left\{\sum_{i=1}^{n-1}(I_0 - I_i), 0\right\}, n = 3,5,7 \quad (2)$$

Where I_0 is the grayscale value of the pixel in the center of the detection structure, I_i is the grayscale value of the pixel numbered i in the detection structure. Taking a 7*7 detection structure as an example, each pixel is numbered in the order as shown in Fig. 5.

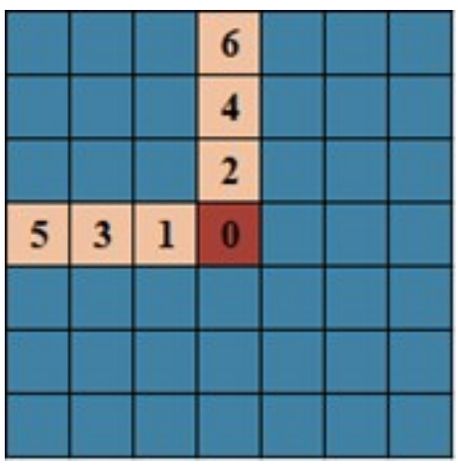

Fig. 5　structure of left associate upper direction, with size of 7*7

图5　7*7大小的上左联合方向检测结构

According to Eq. (2), in each joint direction, the associated gradient is extracted using three different scales of 3*3, 5*5 and 7*7 detection structures, and the maximum value of the multi-scale calculation result is selected as the gradient response of the current pixel in the joint direction:

$$G^1_{max} = \max(G^1_{3*3}, G^1_{5*5}, G^1_{7*7}) \quad (3)$$
$$G^2_{max} = \max(G^2_{3*3}, G^2_{5*5}, G^2_{7*7}) \quad (4)$$
$$G^3_{max} = \max(G^3_{3*3}, G^3_{5*5}, G^3_{7*7}) \quad (5)$$
$$G^4_{max} = \max(G^4_{3*3}, G^4_{5*5}, G^4_{7*7}) \quad (6)$$

where G^i_{n*n} denotes the associated gradient of the current pixel in direction-i shown in Fig. 3 for a detection window of size n*n.

Define the product of the gradients in the four associated directions as the associated directional gradient (ADG) of the current pixel point:

$$ADG = G^1_{max} * G^2_{max} * G^3_{max} * G^4_{max} \quad (7)$$

Since the product is used in the calculation of ADG, when there are multiple targets in one image and the target grayscale difference is large, the product operation will further enlarge the grayscale difference between different targets, making the threshold segmentation phase very difficult. In order to effectively reduce the gradient gap between different targets, a nonlinear function is used to map the ADG to reduce the feature-response gap between different targets. The structural clutter and noise in the background has a very low response in the ADG. To avoid low values of clutter being mapped to high values, a low value truncation of the ADG is performed using Eq. (8) before the nonlinear mapping.

$$ADG_T(x,y) = \begin{cases} ADG(x,y), & ADG(x,y) \geqslant \alpha * Max_{ADG} \\ 0, & ADG(x,y) < \alpha * Max_{ADG} \end{cases} \quad (8)$$

Where Max_{ADG} is the maximum value among all elements of ADG matrix, and α is a coefficient. By the simulation calculation of extreme cases, it can be obtained that α taking 0.1 can better balance the effect of noise elimination and complete retention of multiple targets. Then normalize ADG_T with Eq. (9) to obtain ADG_N and perform ADG_N a nonlinear mapping as Eq. (10).

$$ADG_N(x,y) = \frac{ADG_T(x,y) * 255}{\max(ADG_T)} \quad (9)$$

$$ADG_{mapped}(x,y) = 255 * \frac{\ln(1 + 255 * ADG_N(x,y))}{\ln(1 + 255)}, (x,y) \in ADG \quad (10)$$

Fig. 6 shows the grayscale differences between different targets before and after the nonlinear mapping. Comparing Fig. 6 (c) and Fig. 6 (e), it can be seen that after the nonlinear mapping, the grayscale difference between targets becomes significantly smaller.

1.2　Mean-Contrast based on eliminating isolated noise

Due to the characteristics of the imaging mecha-

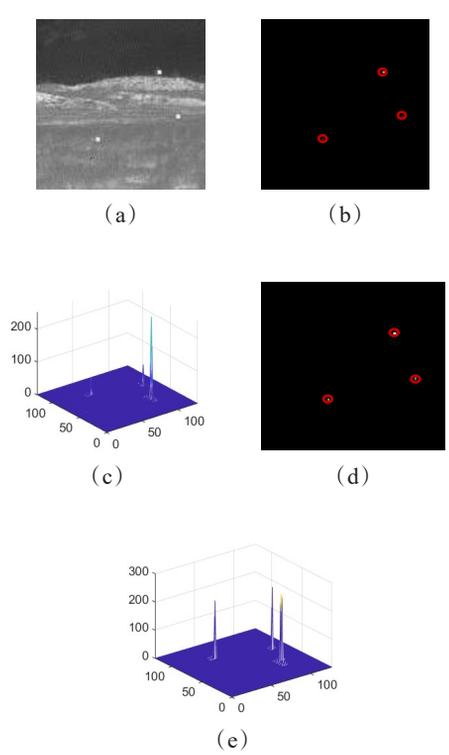

Fig.6　Comparison before and after nonlinear mapping (a) original infrared image, (b) ADG, (c) 3D grayscale view of ADG, (d) $ADG_{mapped}(x,y)$, (e) 3D grayscale view of $ADG_{mapped}(x,y)$

图6　非线性映射前后对比 (a)原始红外图像, (b) ADG, (c) ADG的三维灰度图, (d) ADGmappedx,y, (e) ADGmappedx,y的三维灰度图

nism, there is often a large amount of isolated noise in infrared images. Various smoothing filters are the most common means to eliminate isolated noise in image processing. In this paper, the idea of mean-contrast filtering is combined with the concept of local contrast, and a mean contrast filter structure is designed as shown in Fig. 7, where T is the target region and B_i is the background region.

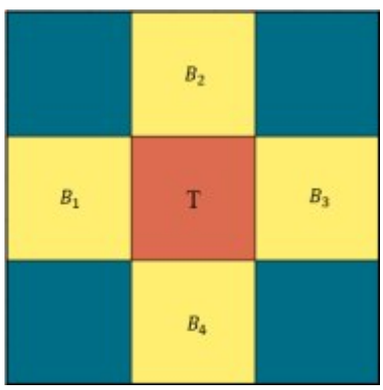

Fig. 7 structure of mean contrast filter
图7 均值滤波结构

When the size of the target region T is n*n, the contrast between the target region T and the background region B_i is defined as Eq. (11).

$$contrast^{i}_{n*n} = \max\left(\frac{\sum_{(x,y)\in T} Img(x,y) - \sum_{(x,y)\in B_i} Img(x,y)}{n*n}, 0\right), \quad (11)$$

Infrared small targets are centered on the brightest point, and the grayscale value decreases in a radial fashion in all directions. Therefore, the maximum contrast value can be obtained when the small targets are exactly or mostly in the T-zone of the detection structure shown in Fig. 7. To accommodate targets of different sizes, multiscale is set in the target region T. For each B_i, the maximum value of the multiscale response is used as the contrast response between B_i and T:

$$contrast_{B_1} = \max(contrast^{1}_{3*3}, contrast^{1}_{5*5}, contrast^{1}_{7*7}), \quad (12)$$

$$contrast_{B_2} = \max(contrast^{2}_{3*3}, contrast^{2}_{5*5}, contrast^{2}_{7*7}), \quad (13)$$

$$contrast_{B_3} = \max(contrast^{3}_{3*3}, contrast^{3}_{5*5}, contrast^{3}_{7*7}), \quad (14)$$

$$contrast_{B_4} = \max(contrast^{4}_{3*3}, contrast^{4}_{5*5}, contrast^{4}_{7*7}), \quad (15)$$

Since some structural noise only has high contrast in some directions, while the infrared small target has similar contrast in all directions, so select the minimum value among $contrast_{B_1}$、$contrast_{B_2}$、$contrast_{B_3}$、$contrast_{B_4}$ as the contrast between the target region and the surrounding neighborhood, which can effectively filter the structural noise and further reduce the potential false alarm rate of the algorithm. The mean-contrast (MC) of the final background region T is defined as Eq. (16).

$$MC = \min\{contrast_{B_1}, contrast_{B_2}, contrast_{B_3}, contrast_{B_4}\}. \quad (16)$$

1.3 Calculation of the algorithm

After obtaining the ADG_{mapped} and the MC, the final result obtained by the algorithm based on the association directional gradient and the mean contrast ($ADGMC$) is defined as

$$ADGMC = ADG_{mapped} * MC. \quad (17)$$

1.4 Threshold segmentation

A new image matrix can be obtained after calculating the $ADGMC$ for the original infrared image. As the calculation of ADG_{mapped} involves a threshold truncation operation to eliminate a large amount of noise in the background, and the multiplication operation of two feature maps further reduces the possibility of false alarms of the algorithm, it is only necessary to determine the threshold value based on the maximum value in $ADGMC$ to obtain a better detection effect. The threshold T is defined as in Eq. (18):

$$T = \beta * Max_{ADGMC}, \quad (18)$$

Where Max_{ADGMC} is the maximum value among all elements of the $ADGMC$ matrix, β is the coefficient between 0 and 1. Experiments have shown that β taking values between 0.4 and 0.6 can better complete the target detection tasks under various scenarios such as single target and multi-target.

The final segmentation result $Binary_{(x,y)}$ is obtained by Eq. (19).

$$Binary_{(x,y)} = \begin{cases} 0, GC_{(x,y)} \geqslant T \\ 1, GC_{(x,y)} < T \end{cases}, \quad (19)$$

2 Experiments and results

In this section, firstly, the advantage of associated directional gradient over single direction gradient is verified. Secondly, the suppression effect of mean contrast proposed on independent noise and structural background is verified. Finally, the algorithm proposed in this paper is applied to four real single-target infrared image sequences and a single-frame infrared image group to analyze the performance of the algorithm and compare it with other algorithms. The image data are described in detail in Table 1. The experiments were done on a computer configured with an Intel(R) Core(TM) i5-4460 CPU @ 3.20 GHz 3.20 GHz.

Table 1 Detailed description of image data
表1 图像数据的详细描述

	size	amount	target number	data type
Data1	320*240	100	100	single-target sequence
Data2	320*240	30	30	single-target sequence
Data3	320*240	100	100	single-target sequence
Data4	320*240	100	100	single-target sequence
Data5	127*127	21	26	mixed image group

2.1 Experimental procedure and results

2.1.1 Validation of the associated directional gradient module

Fig. 8 shows an example of the "target close to the highlighted edge" case described above. It contains three

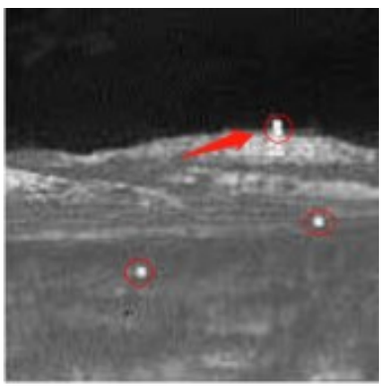

Fig. 8　test image
图 8　测试图像

small targets, with the lower side of the target indicated by the arrow being close to the highlighted edge. The associated directional gradient features and the four individual directional gradient features are computed separately, and the results are shown in Fig. 9:

From Fig. 9(c), it can be seen that the return value of the single-direction gradient below the target is almost zero because the target is close to the highlighted edge; whereas the return value of the associated directional gradient is related to the surrounding adjacent gradient, so in Fig. 9(i), the return value of the associated directional gradient of the small target near the highlighted edge is still more obvious. Comparing the product of the four directional gradients in the two ways, we can see that combining the two adjacent directional gradients into the joint directional gradient can eliminate the effect of the highlighted edge on the detection of small infrared targets. Comparing the results of the product of the gradients in the four directions under the two gradient calculation methods in Fig. 9(f) and Fig. 9(m), it can be seen that binding the gradients in two adjacent directions as associated directional gradients can eliminate the effect of the highlighted edges on the detection of small IR targets.

2.1.2　Validation of the mean contrast module

As shown in Fig. 10, the red boxes are small infrared targets, and the red circles are marked with artificially added isolated noise.

Calculate the *MC* for Fig. 10 to obtain Fig. 11. Fig. 11(a) to Fig. 11(d) correspond to the mean contrast in the upper, down, left, and right directions, respectively. Fig. 11(e) is the result of taking the minimum value of the mean contrast in four directions.

From Fig. 11(a) to Fig. 11(d), it can be seen that the isolated noise is eliminated due to the mean filter structure used in the calculation of *MC*, and the structural background, such as the cloud boundary, has different contrast in each direction. Fig. 11(e) shows the result of taking the minimum value of the mean contrast in four directions. Since the small target has a high contrast in all directions, while the structural background has a large difference in contrast in different directions, the operation of taking the minimum value can eliminate most of the structural background while having no effect on the small target.

Fig. 12 shows the results of calculating the *ADGMC* for Fig. 10. From Fig. 12(b) and Fig. 12(c), it can be seen that during the calculation of *ADG*, the isolated noise is also significantly enhanced along with the target, which undoubtedly affects the detection results. Using Fig. 11(e) to multiply with Fig. 12(d) to obtain Fig. 12(e), *ADGMC*. As can be seen from the Fig. 12(e), the isolated noise is completely suppressed.

2.1.3　Experiment on infrared data

In this section, the *ADGMC* algorithm is applied to the real IR images listed in Table I. The processing pro-

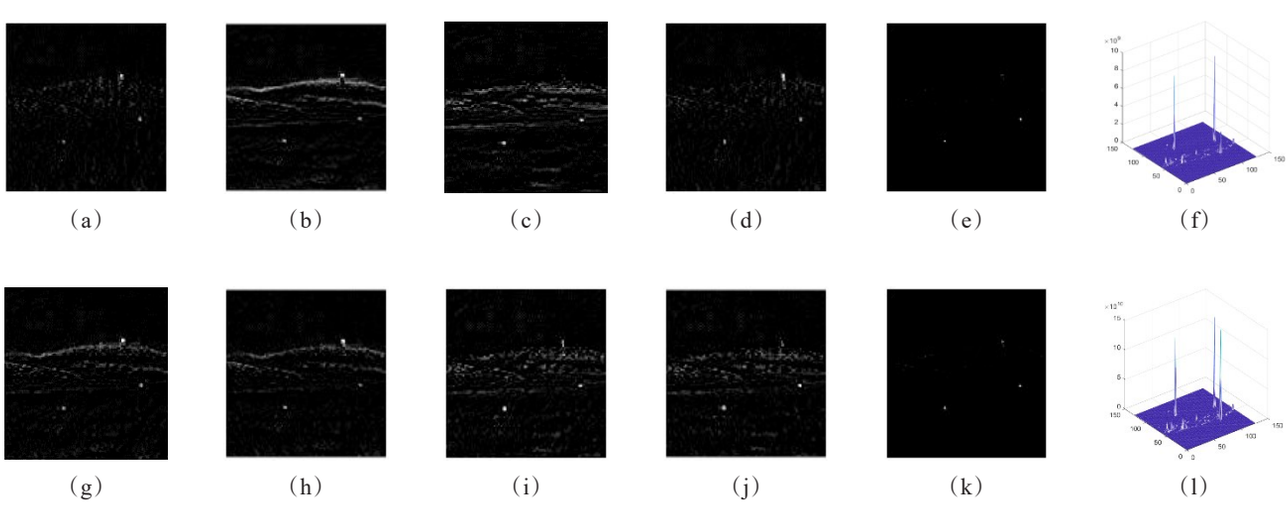

Fig.9　Comparison of assoicated directional gradient and single directional gradient (a) left gradient, (b) upper gradient, (c) down gradient, (d) right direction, (e) single-direction gradient product, (f) mesh of (e), (g) left-upper gradient, (h) upper-right gradient, (i) down-left gradient, (j) right-down gradient, (k) associated directional gradient product, (l) mesh of (k)
图 9　联合方向梯度与单方向梯度对比 (a) 左方梯度, (b) 上方梯度, (c) 下方梯度, (d) 右方梯度, (e) 单向梯度乘积图, (f) (e)的 mesh 图, (g) 左上方联合梯度, (h) 上右方联合梯度, (i) 下左方联合梯度, (j) 右下方联合梯度, (k) 联合放 i 像梯度乘积图, (l) (k)的 mesh 图

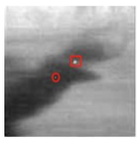

Fig. 10 IR image with isolated noise added
图10 添加了孤立噪声的红外图像

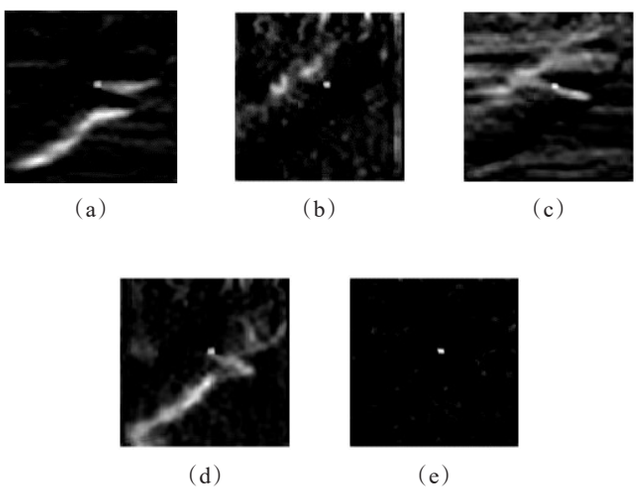

Fig. 11 MC calculation process diagram (a) left mean contrast; (b) upper mean contrast; (c) down mean contrast; (d) right mean contrast; (e) final MC
图11 均值对比度计算过程图 (a)左方均值对比度,(b)上方均值对比度,(c)下方均值对比度,(d)右方均值对比度,(e)最终均值对比度输出

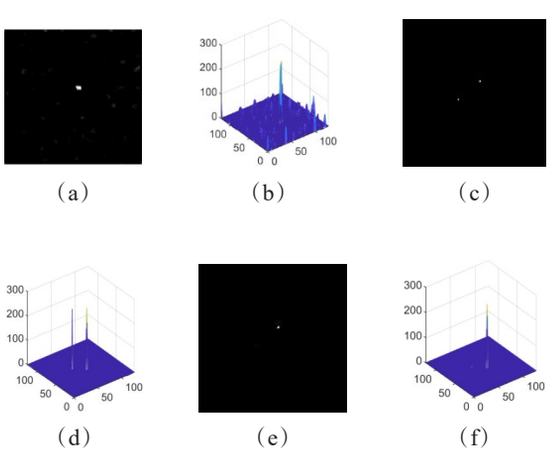

Fig.12 Diagram of *ADGMC* calculation process (a) grayscale diagram of *MC*; (b) mesh of *MC*; (c) grayscale diagram of *ADG*; (d) mesh of *ADG*; (e) grayscale diagram of *ADGMC*; (f) mesh of *ADGMC*
图12 ADGMC计算过程图 (a) MC的灰度图,(b) MC的mesh图,(c) ADG的灰度图,(d) ADG的mesh图,(e) ADGMC的灰度图,(f) ADGMC的mesh图

cess of each single-target image sequence (Data1-Data4) by the *ADGMC* algorithm is shown in Fig. 13. Fig. 13(a) shows the original infrared image, which contains scenes of sky, ocean, bright and dark backgrounds, near the highlighted edge, and multiple targets. Fig. 13(b) and Fig. 13(c) correspond to the *ADG* and ADG_{mapped}, respectively. By comparing the two figures, it can be seen that after nonlinear mapping, the low-value pixel points in the image are mapped to higher values, and the grayscale difference between multiple real targets becomes smaller, which is more conducive to the complete detection of small targets. Fig. 13(d) shows the *MC* calculation results, and it can be seen that there is isolated noise with higher response in ADG_{mapped}, which is suppressed to some extent in the *MC* calculation. Fig. 13(e) is the final *ADGMC* image, which is obtained by multiplying ADG_{mapped} and *MC*. Fig. 13(f) shows the detection results after threshold segmentation. Data5 is used as a supplementary experiment to verify the robustness of the algorithm in a variety of scenes, and Fig. 14 shows the detection results with the forest as the background in data5. The comprehensive experimental results show that the algorithm proposed in this paper can adapt to a variety of scenes such as sky, ocean, and forest to accomplish the task of infrared weak target detection.

2.2 Performance comparison of algorithms

In this section, four general evaluation metrics, signal-to-clutter ratio gain (SCRG), background suppression factor (BSF), receiver operating characteristic curve (ROC) and algorithm runtime efficiency, are chosen to compare the algorithm proposed in this paper with some classical algorithms and current advanced algorithms, including AAGD, AMWLCM, LEF, Max-mean, Max-med, MPCM, Top-hat, RLCM, TLLCM.

2.2.1 Signal-to-clutter ratio gain

The signal-to-clutter ratio (SCR) describes how difficult it is to detect small infrared targets. The higher SCR the easier the target is to detect. SCR is defined as.

$$SCR = \frac{|\mu_t - \mu_b|}{\sigma_b}, \quad (20)$$

where μ_t denotes the average pixel value of the target, the σ_b and μ_b denote the standard deviation and mean pixel values of the adjacent regions.

To assess the ability of the algorithm to enhance the target, the SCRG is defined as

$$SCRG = \frac{SCR_{out}}{SCR_{in}}, \quad (21)$$

Where the SCR_{out} and SCR_{in} denote the SCR of the processed image and the original infrared image. A larger SCRG value means that more information about the target is extracted from the original image, indicating that the algorithm has better enhancement capability for the target. In the comparison experiments, the mean SCRG values of single-frame images corresponding to each algorithm are shown in Table 2, with the bolded representing the optimal performance. It can be seen that the algorithms proposed in this paper exhibit optimal target enhancement capability under each set of image data.

2.2.2 Background suppression factor

The BSF is used to assess the ability of various detection methods to suppress background noise. Generally, the higher the BSF, the better the algorithm's ability

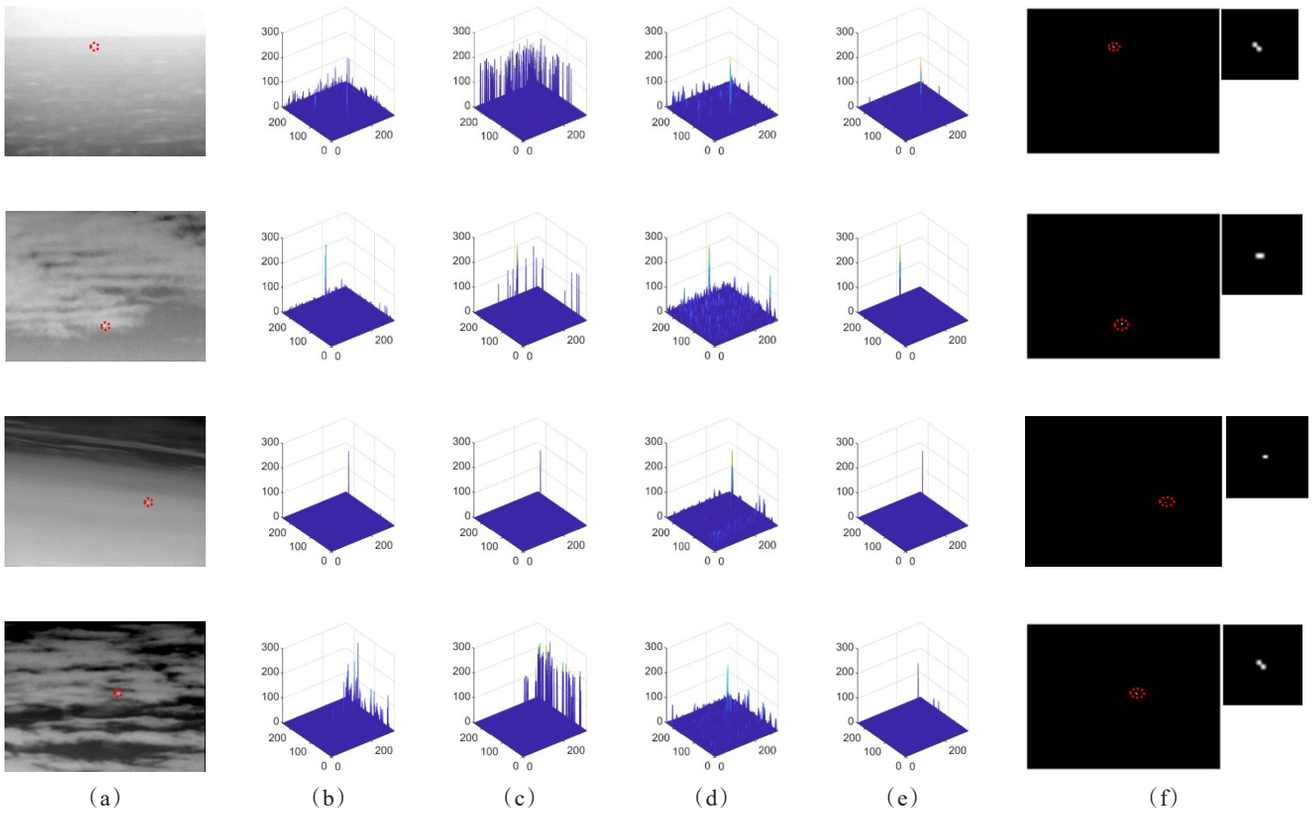

Fig. 13　top to bottom: Data1-Data4 (a) original image, (b)*ADG*, (c) ADG_{mapped}, (d) *MC*, (e) *ADGMC*, (f) Result(The top right corner is a zoomed-in view near the small target)
图 13　从上到下对应 Data1-Data4 (a)原始图像,(b) ADG,(c) ADGmapped ,(d) MC,(e) ADGMC,(f)阈值分割结果(右上角是目标附近区域放大图)

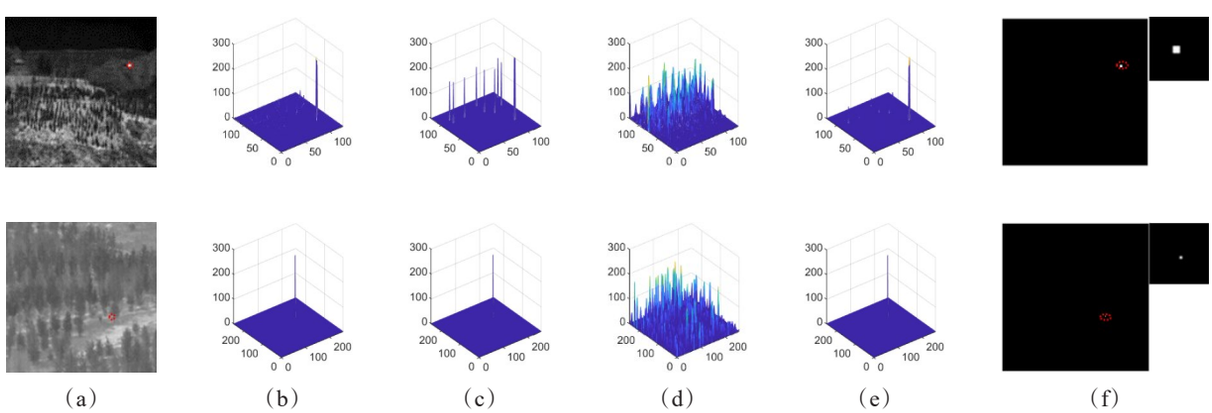

Fig. 14　Part of Data5 processing process (a) original image, (b)*ADG*, (c) ADG_{mapped}, (d) *MC*, (e) *ADGMC*, (f) Result(The top right corner is a zoomed-in view near the small target)
图 14　Data5 部分数据的处理过程图 (a)原始图像,(b) ADG,(c) ADGmapped,(d) MC,(e) ADGMC,(f)阈值分割结果(右上角是目标附近区域放大图)

to suppress background noise. This is defined as follows.

$$BSF = \frac{\sigma_{in}}{\sigma_{out}} \quad , \quad (22)$$

where σ_{in} and σ_{out} represent the Standard Deviation of the background area (the whole image except the target area) in the original image and the image after processing by each algorithm, respectively.

In the comparison experiments, the mean BSF values of the single image corresponding to each algorithm are shown in Table 3. The bolded represents the optimal performance. It can be seen that the algorithms proposed in this paper exhibit optimal background noise suppres-

Table 2 Average SCRG results for different detection methods for each group of images
表2 不同算法计算各组图像数据对应的平均SCRG

	AAGD	AMWLCM	LEF	Maxmean	Maxmed	MPCM	Tophat	RLCM	TLLCM	Proposed
Data1	4.99	1.00	1.58	0.53	2.55	1.26	1.20	0.08	1.19	**38.66**
Data2	3.37	1.09	1.72	0.74	0.37	2.32	1.58	0.34	4.38	**48.28**
Data3	1.91	0.46	1.45	0.64	0.39	1.40	1.23	0.45	2.47	**74.34**
Data4	5.64	0.18	3.21	0.49	0.20	3.21	0.73	0.49	15.77	**125.42**
Data5	5.23	1.22	2.61	0.68	0.52	3.08	1.28	0.27	8.07	**21.37**

sion under all sets of image data.

2.2.3 Receiver operating characteristic curve

The ROC can quantitatively describe the dynamic relationship between False Positive Rate (FPR) and True Positive Rate (TPR). In the performance evaluation of infrared small target detection, TPR and FPR are defined as

$$\mathrm{TPR} = \frac{\text{number of targets detected}}{\text{number of actual targets}}, \quad (23)$$

$$\mathrm{FPR} = \frac{\text{number of false target pixels}}{\text{total number of pixels in the original image}}, \quad (24)$$

The larger the area under the ROC curve (AUC), the better the detection performance of the corresponding algorithm, which is represented in the ROC curve graph by the concentration of the coordinate points in the upper-left corner area of the image. The ROC curves for the different detection methods for each group of images in the experiment are shown in Fig. 15. It can be seen that under various thresholds, the false alarm rate of the method proposed in this paper remains at a low level for both single-target sequences and multi-target complex image groups, while the detection rate is higher, highlighting the superiority of the algorithm in this paper.

2.2.4 Time efficiency

The performance of an algorithm in terms of time is one of the criteria used to evaluate it. The average time efficiency for single-frame image detection in the comparison experiments is shown in Table 4. The algorithm proposed is not as fast as the classical background subtraction method due to the multiple scales used to accommodate targets of different sizes. The TLLCM algorithm has excellent time efficiency, but it does not perform as well as the proposed method in other evaluation metrics such as SCRG, BSF, etc. The background noise and the enhanced target can hardly be suppressed by using a single filter to estimate the background. Moreover, the time efficiency of the proposed method is controlled to the order of hundredths of a second, which is sufficient for various scenarios.

3 Conclusion

In this letter, a new method for infrared small target detection called *ADGMC* is proposed. A new feature detection structure with associated directional gradients has been designed in the associated directional gradient module, and a contrast detection structure incorporating directional information and the idea of mean filtering has been designed in the mean contrast module. Both modules can effectively avoid the influence of high-intensity edges on the gradient variation pattern of small target models. In addition, a non-linear mapping function has introduced into infrared small target detection to ensure the method can complete the detection of all targets in multi-target scenarios. The experimental results show

Table 3 Average BSF results for different detection methods for each group of images
表3 不同算法计算各组图像数据对应的平均DSF

	AAGD	AMWLCM	LEF	Maxmean	Maxmed	MPCM	Tophat	RLCM	TLLCM	Proposed
Data1	36.69	8.35	19.62	9.94	16.52	32.88	6.62	4.96	21.82	**46.12**
Data2	8.02	1.28	2.83	1.11	1.27	5.30	1.42	2.39	5.84	**12.38**
Data3	8.59	3.85	3.93	3.30	4.39	8.73	2.11	5.35	9.45	**33.92**
Data4	18.28	1.96	9.87	1.94	2.02	17.27	1.77	5.35	12.28	**23.76**
Data5	8.31	2.31	6.08	2.63	2.74	7.15	2.43	2.23	5.79	**12.93**

Table 4 Average time efficiency of different detection methods for each group of images (in s)
表 4 不同算法计算各组图像数据对应的平均时间

秒

	AAGD	AMWLCM	LEF	Maxmean	Maxmed	MPCM	Tophat	RLCM	TLLCM	Proposed
Data1	0.042 9	2.819 1	8.042 3	0.006 1	0.008 9	0.041 8	3.052 2	1.947 1	**0.004 2**	0.040 1
Data2	0.039 4	2.801 2	8.048 2	0.006 0	0.011 2	0.041 5	3.615 1	2.378 0	**0.003 7**	0.040 1
Data3	0.039 7	2.806 9	8.047 4	0.005 9	0.008 8	0.042 2	3.454 3	2.257 3	**0.003 8**	0.041 1
Data4	0.038 9	2.802 7	8.012 9	0.005 9	0.009 9	0.041 6	3.621 3	2.377 2	**0.003 8**	0.042 2
Data5	0.080 1	1.657 7	5.866 0	**0.012 3**	0.010 4	0.065 5	2.767 7	2.206 9	0.017 5	0.013 8

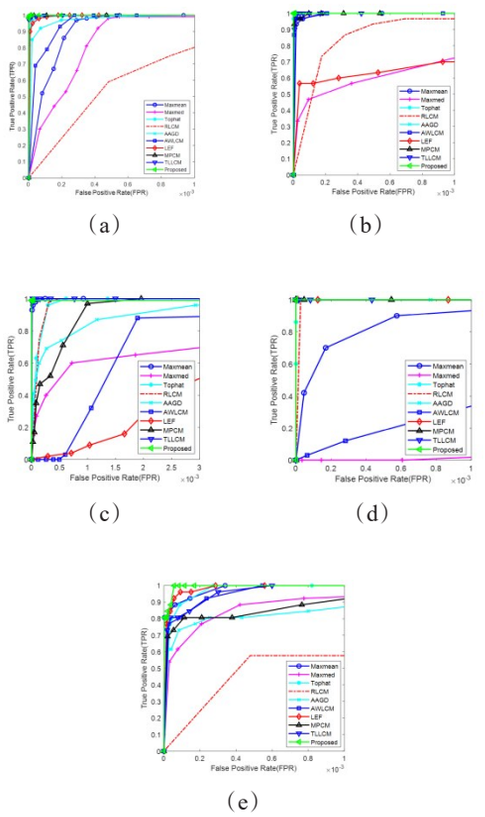

Fig. 15　Data1 to Data5 corresponding ROC curves (a) Data 1, (b) Data 2, (c) Data 3, (d) Data 4
图 15　Data1 至 Data5 对应的 ROC 曲线 (a)Data 1, (b)Data 2, (c) Data 3, (d)Data 4

that *ADGMC* has strong target-enhancement and background-suppression capabilities, especially for scenes with high intensity edges and multiple targets.

References

[1] M. Zhao, W. Li, L. Li, J. Hu, P. Ma and R. Tao, "Single-Frame Infrared Small-Target Detection: A survey," *in IEEE Geoscience and Remote Sensing Magazine*, vol. **10**, no. 2, pp. 87-119, June 2022, doi: 10.1109/MGRS.2022.3145502.

[2] Zhang K , Ni S , Yan D , *et al*. Review of Dim Small Target Detection Algorithms in Single-frame Infrared Images[C]// 2021 IEEE 4th Advanced Information Management, Communicates, Electronic and Automation Control Conference (IMCEC). 0.

[3] Deng, He, Zhou, et al. Entropy-based window selection for detecting dim and small infrared targets[J]. *Pattern Recognition: The Journal of the Pattern Recognition Society*, 2017, **61**:66-77.

[4] S. Huang, Z. Peng, Z. Wang, X. Wang and M. Li, "Infrared Small Target Detection by Density Peaks Searching and Maximum-Gray Region Growing," *in IEEE Geoscience and Remote Sensing Letters*, vol. **16**, no. 12, pp. 1919-1923, Dec. 2019, doi: 10.1109/LGRS.2019.2912989.

[5] C. Xia, X. Li, L. Zhao and R. Shu, "Infrared Small Target Detection Based on Multiscale Local Contrast Measure Using Local Energy Factor," *in IEEE Geoscience and Remote Sensing Letters*, vol. **17**, no. 1, pp. 157-161, Jan. 2020, doi: 10.1109/LGRS.2019.2914432.

[6] Y. Shi, Y. Wei, H. Yao, D. Pan and G. Xiao, "High-Boost-Based Multiscale Local Contrast Measure for Infrared Small Target Detection," *in IEEE Geoscience and Remote Sensing Letters*, vol. **15**, no. 1, pp. 33-37, Jan. 2018, doi: 10.1109/LGRS.2017.2772030.

[7] H. Deng, X. Sun, M. Liu, C. Ye and X. Zhou, "Infrared small-target detection using multiscale gray difference weighted image entropy," *in IEEE Transactions on Aerospace and Electronic Systems*, vol. **52**, no. 1, pp. 60-72, February 2016, doi: 10.1109/TAES.2015.140878.

[8] Suyog D. Deshpande, Meng Hwa Er, Ronda Venkateswarlu, Philip Chan, "Max-mean and max-median filters for detection of small targets," Proc. *SPIE* 3809, Signal and Data Processing of Small Targets 1999, (4 October 1999); https://doi.org/10.1117/12.364049

[9] Ming Zeng, Jianxun Li, Zhang Peng, The design of Top-Hat morphological filter and application to infrared target detection, Infrared Physics & Technology, Volume 48, Issue 1, 2006, Pages **67**-76, ISSN 1350-4495, https://doi.org/10.1016/j.infrared.2005.04.006.

[10] Xiangzhi Bai, Fugen Zhou, Analysis of new top-hat transformation and the application for infrared dim small target detection, Pattern Recognition, Volume 43, Issue 6, 2010, Pages **2145**-2156, ISSN 0031-3203, https://doi.org/10.1016/j.patcog.2009.12.023.

[11] JIE LIU, ZIQING HE, ZUOLONG CHEN, *et al*. Tiny and Dim Infrared Target Detection Based on Weighted Local Contrast [J]. *IEEE geoscience and remote sensing letters*, 2018, **15**(11): 1780-1784. doi: 10.1109/LGRS.2018.2856762.

[12] J. Han *et al*., "Infrared Small Target Detection Based on the Weighted Strengthened Local Contrast Measure," *in IEEE Geoscience and Remote Sensing Letters*, vol. **18**, no. 9, pp. 1670-1674, Sept. 2021, doi: 10.1109/LGRS.2020.3004978.

[13] J. Han, S. Moradi, I. Faramarzi, C. Liu, H. Zhang and Q. Zhao, "A Local Contrast Method for Infrared Small-Target Detection Utilizing a Tri-Layer Window," *in IEEE Geoscience and Remote Sensing Letters*, vol. **17**, no. 10, pp. 1822-1826, Oct. 2020, doi: 10.1109/LGRS.2019.2954578.

[14] J. Han, K. Liang, B. Zhou, X. Zhu, J. Zhao and L. Zhao, "Infrared Small Target Detection Utilizing the Multiscale Relative Local Contrast Measure," *in IEEE Geoscience and Remote Sensing Letters*, vol. **15**, no. 4, pp. 612-616, April 2018, doi: 10.1109/LGRS.2018.2790909.

[15] C. L. P. Chen, H. Li, Y. Wei, T. Xia and Y. Y. Tang, "A Local Contrast Method for Small Infrared Target Detection," *in IEEE Transactions on Geoscience and Remote Sensing*, vol. **52**, no. 1, pp. 574-581, Jan. 2014, doi: 10.1109/TGRS.2013.2242477.

[16] J. Han, Y. Ma, B. Zhou, F. Fan, K. Liang and Y. Fang, "A Robust Infrared Small Target Detection Algorithm Based on Human Visual System," *in IEEE Geoscience and Remote Sensing Letters*, vol. **11**, no. 12, pp. 2168-2172, Dec. 2014, doi: 10.1109/LGRS.2014.2323236.

[17] PANSheng-da, ZHANGSu, ZHAO Ming, *etal*. Infrared Small Target Detection Based on Double-layer Local Contrast Measure [J]. *Acta Photonica Sinica*, 2020, **49**(1):0110003

[18] L. Wu, Y. Ma, F. Fan, M. Wu and J. Huang, "A Double-Neighborhood Gradient Method for Infrared Small Target Detection," *in IEEE Geoscience and Remote Sensing Letters*, vol. **18**, no. 8, pp. 1476-1480, Aug. 2021, doi: 10.1109/LGRS.2020.3003267.

[19] G. Qiu, H. Yang, Y. Wei, Y. Wang and P. Luo, "Infrared small target detection based on local multidirectional gradient," *2019 Chinese Automation Congress (CAC)*, 2019, pp. 5679-5683, doi: 10.1109/CAC48633.2019.8997030.

[20] C. Xia, S. Chen and Y. Luo, "Omnidirectional Mirror Gradient Dissimilarity for Infrared Small Target Detection," *IGARSS 2022 - 2022 IEEE International Geoscience and Remote Sensing Symposium*, 2022, pp. 3255-3258, doi: 10.1109/IGARSS46834.2022.9884151.

[21] Zhang H, Zhang L, Yuan D, *et al*. Infrared small target detection based on local intensity and gradient properties[J]. *Infrared Physics & Technology*, 2018, **89**: 88-96.

[22] H. Deng, X. Sun, M. Liu, C. Ye and X. Zhou, "Infrared small-target detection using multiscale gray difference weighted image entropy," *in IEEE Transactions on Aerospace and Electronic Systems*, vol. **52**, no. 1, pp. 60-72, February 2016, doi: 10.1109/TAES.2015.140878.

[23] Saeid Aghaziyarati, Saed Moradi, Hasan Talebi, Small infrared target detection using absolute average difference weighted by cumulative directional derivatives, Infrared Physics & Technology, Volume 101, 2019, Pages **78**-87, ISSN 1350-4495, https://doi.org/10.1016/j.infrared.2019.06.003.